Advances in Water Resources 137 (2020) 103519

Contents lists available at ScienceDirect

Advances in Water Resources

journal homepage: www.elsevier.com/locate/advwatres

A novel 1D-2D coupled model for hydrodynamic simulation of flows in drainage networks

Qian Li [a], Qiuhua Liang [a,b,*], Xilin Xia [a,b]

[a] School of Architecture, Building and Civil Engineering, Loughborough University, Loughborough, UK
[b] International Institute for Hydroinformatics & Hazard Resilience (IIHHR), Hebei University of Engineering, Handan, China

ARTICLE INFO

Keywords:
Drainage networks
Urban flood modelling
Junction calculation
TPA
Shallow water equations
Transient flow

ABSTRACT

Drainage network modelling is often an essential component in urban flood prediction and risk assessment. Drainage network models most commonly use different numerical procedures to handle flows in pipes and junctions. Numerous numerical schemes and models of different levels of complexity have been developed and reported to predict flows in pipes. However, calculation of the flow conditions in junctions has received much less attention and has been traditionally achieved by solving only the continuity equation. This method is easy to implement but it neglects the momentum exchange in the junctions and cannot provide sufficient boundary conditions for the pipe calculation. In this work, a novel numerical scheme based on the finite volume solution to the two-dimensional (2D) shallow water equations (SWEs) is proposed to calculate flow dynamics in junctions, which directly takes into account both mass and momentum conservation and removes the necessity of implementing complicated boundary settings for pipe calculations. This new junction simulation method is then coupled with the widely used two-component pressure approach (TPA) for the pipe flow calculation, leading to a new integrated drainage network model. The new 1D-2D coupled drainage network model is validated against an experimental and several idealised test cases to demonstrate its potential for efficient and stable simulation of flow dynamics in drainage networks.

1. Introduction

Flood inundation models have become an indispensable tool to predict flood dynamics and to evaluate flood impacts in cities. Drainage network modelling is often an integrated component of an urban flood simulation tool. Pipes and junctions are the two essential elements of any sizable urban drainage network and are commonly calculated by different model components in drainage network models. To predict the flow dynamics in pipes, the 1D Saint-Venant equations (or one of the modified/ simplified forms) are often used and solved numerically. In most of the drainage network models, effective approaches have been developed to handle the transitioning free-surface and pressurized flow conditions in pipes that repeatedly happen during an urban flood event. One group of these approaches uses different equations for free-surface and pressurized flows. Examples include the interface tracking model (Wiggert, 1972; Politano et al., 2007), the rigid column-based model (McCorquodale and Hamam,1983; Li and McCorquodale,1999) and the Illinois transient model (ITM) (León et al., 2010a). Another type of widely used approach solves a single set of equations but is incorporated with the numerical calculation schemes to handle pressurised flows. A typical example is the Pressman slot scheme proposed by Preissmann (1961), which has been widely adopted and further developed by many researchers (e.g. Cunge et al., 1980; Capart et al., 1997; Trajkovic et al., 1999; Malekpour and Karney, 2014; Maranzoni et al., 2015; Noh et al., 2016). An alternative method called the two-component pressure approach (TPA) was also proposed and reported by Vasconcelos et al. (2006, 2007) for simulating transient flows. TPA models assume that the pipe walls are elastic and subsequently the cross-sectional area of a pipe may expand when the flow inside is pressurized. TPA models can effectively simulate various types of unsteady flows including free-surface flow, mixed flow (partly gravity-partly pressurized flow), pressurized flow, sub-atmospheric pressure flow as well as flow transitions (Bousso et al., 2012).

The calculation of junction flows, however, has received much less attention despite the fact that they are an integrated part of a drainage network model and are essential to provide the necessary boundary conditions (BCs) for accurate calculation of pipe flows. The traditional approach for the junction flow calculation neglects momentum conservation and considers only the continuity equation to estimate junction water depth. Such an approach has been widely used in drainage modelling and implemented in SWMM (SWMM manual; Hsu et al., 2000; Burger et al., 2014) and many other urban drainage

* Corresponding author at: School of Architecture, Building and Civil Engineering, Loughborough University, Loughborough, UK.
E-mail address: q.liang@lboro.ac.uk (Q. Liang).

https://doi.org/10.1016/j.advwatres.2020.103519
Received 13 April 2019; Received in revised form 18 January 2020; Accepted 20 January 2020
Available online 21 January 2020

models (e.g., Schmitt et al., 2005; Chang et al., 2015; Noh et al., 2016, 2018; Leandro and Martins, 2016). Although this traditional approach may be computationally efficient, it normally requires additional complicated methods to provide sufficient BCs for transient flow calculations in pipes. For example, a decision tree method was implemented by Capart et al. (1999) at the interfaces between junctions and pipes to illustrate possible boundary flow regimes. Sanders and Bradford (2010) extended this work and developed an improved framework to include different types of BCs for free-surface and pressurized flows. A similar effort has also been made in modelling the flow around an island in a river where the flow connections around the island are represented as junctions/bifurcations to provide inner BCs to connect with the river flow (Franzini et al., 2018). However, these approaches require identification of various BCs according to the flow variables (e.g. Froude number, water level, dryness tolerance, etc.) at each time step, which is difficult to implement and may affect the computational efficiency and numerical stability of the overall drainage model. León et al. (2010b) proposed a junction and drop-shaft BC model, which was coupled to an ITM for the simulation of mixed flows in pipes. Separate Ordinary Differential Equations (ODEs) derived from conservation of mass and momentum have been also used for estimating junction flows (Borsche and Klar, 2014). However, the resulting approaches are complicated and computationally inefficient as a varying number of equations must be solved at each junction according to the connecting pipes and flow conditions.

Computational fluid dynamics (CFD) models have also been adopted to simulate the complex flow dynamics including turbulence and vorticity inside junctions (Beg et al., 2017, 2018). However, these models are considered to be over-sophisticated for an urban-scale drainage flow simulation where the localised fluid structures will have limited influence on the broad-scale flow dynamics. Furthermore, the lack of detailed junction data makes the computationally expensive effort of little practical value. Preliminary attempts have also been made to use 3D (Hong and Kim, 2011) or 2D (Bermúdez et al., 2017; Herty and Seaïd, 2008) domains to idealize junction nodes in gas pipe network modelling. However, such an approach has not been investigated in modelling storm water drainage networks.

As a summary, the current numerical methods for junction flow calculations suffer from various numerical restrictions and further research is needed to develop alternative approaches to support accurate and computationally efficient drainage modelling for large-scale real-world applications. This paper aims to develop and present an innovative strategy by treating the drainage junctions as 2D free surface domains. Taking into account mass and momentum conservation, the new junction calculation model predicts water depth and flow rate to automatically provide complete BCs for the pipe flow calculations. The new 2D junction model is then coupled with a TPA model to develop a new 1D-2D coupled drainage network modelling system. The rest of the paper is organized as follow: Section 2 introduces the numerical models for the 1D pipe and 2D junction calculations; the new coupled drainage model is tested and validated in Section 3; finally, brief conclusions are drawn in Section 4.

2. New 1D-2D coupled drainage network model

In this section, the proposed 1D-2D coupled model for simulating transient flows in drainage networks will be introduced in detail.

2.1. Pipe model

To implement a TPA model for calculating transitioning flows in pipes, the Saint-Venant equations are extended to simulate both free-surface and pressurized flows (Vasconcelos et al., 2006) and can be written in the matrix form of 1D conservation laws as:

$$\frac{\partial \mathbf{U}_P}{\partial t}+\frac{\partial \mathbf{F}_P}{\partial x}=\mathbf{S}_{Pb}+\mathbf{S}_{Pf} \tag{1}$$

$$\mathbf{U}_P=\begin{bmatrix}A\\ Q_P\end{bmatrix},\mathbf{F}_P=\begin{bmatrix}Q_P\\ Q_P^2/A+I\end{bmatrix},\mathbf{S}_{Pb}=\begin{bmatrix}0\\ -gA\frac{dz}{dx}\end{bmatrix},\mathbf{S}_{Pf}=\begin{bmatrix}0\\ -c_D\frac{PQ_P|Q_P|}{A^2}\end{bmatrix} \tag{2}$$

where the subscripts P, b and f respectively represent 'pipe', 'bed' and 'friction'; t denotes the time; x is the longitudinal coordinate along the pipe direction; A is the cross-sectional area; Q_P is the flow discharge; z is the bottom elevation of the pipe above an arbitrary datum; $c_D=gn_P^2R_P^{-1/3}$ is the roughness coefficient with n_P being the Manning coefficient and R_P being the hydraulic radius; P is the wetted perimeter; and I is the pressure term.

Specifically, the pressure term I must be calculated differently for free-surface and pressurised flow conditions. Under the free-surface flow conditions, I is normally calculated by$I=pA/\rho$ with p being the fluid pressure at the centroid of cross-sectional area and ρ being the fluid density, which may be expanded to become:

$$I(\theta)=\frac{1}{24}\left[3\sin(\theta/2)-\sin^3(\theta/2)-3(\theta/2)\cos(\theta/2)\right]gd^3 \tag{3}$$

where g is the gravitational acceleration, d is the pipe diameter and θ is the wetted angle related to the water depth h_p:

$$\theta=2\arccos\left(1-2h_p/d\right). \tag{4}$$

Related to θ, the geometrical variables A and top width T are given by

$$A=\frac{1}{8}(\theta-\sin\theta)d^2 \tag{5}$$

$$T=d\sin\left(\frac{\theta}{2}\right) \tag{6}$$

based on which the gravity wave celerity in a pipe is defined as:

$$c=\sqrt{\frac{gA}{T}}=\sqrt{\frac{gd(\theta-\sin\theta)}{8\sin(\theta/2)}}. \tag{7}$$

The variables A, T and c are used in the calculation of numerical fluxes, which will be introduced in more detail in the next section.

When the flow is under pressurized flow conditions, a different pressure term related to the surcharge head can be obtained by assuming an elastic pipe wall, and I may be accordingly estimated using

$$I(H)=\frac{\pi}{4}gd^2(H+d/2) \tag{8}$$

in which H is the pressurized head calculated by

$$H=\frac{a^2}{g}\left(\frac{A-A_P}{A_P}\right) \tag{9}$$

where a is the acoustic wave speed and A_p is the original cross-sectional area of the pipe under consideration.

The above 1D TPA governing Eqs. (1) and (2) are numerically solved using a first-order Godunov-type finite volume scheme. The 1D computational domain (i.e. each of the pipes in a network) is discretised using uniform grids. In an arbitrary cell i, the following finite volume time-marching formula is used to update the flow variables from time level n to $n+1$:

$$\mathbf{U}_{Pi}^{n+1}=\mathbf{U}_{Pi}^{n}-\frac{\Delta t}{\Delta x}\left[\mathbf{F}_{i+1/2}^{n}-\mathbf{F}_{i-1/2}^{n}\right]+\Delta t\left(\mathbf{S}_{Pbi}^{n}+\mathbf{S}_{Pfi}^{n+1}\right) \tag{10}$$

in which Δx is the cell length; Δt is the time step; $\mathbf{F}_{i+1/2}^{n}$ and $\mathbf{F}_{i-1/2}^{n}$ are the numerical fluxes across the right and left cell interfaces; $\mathbf{S}_{Pbi}^{n}$ and $\mathbf{S}_{Pfi}^{n+1}$ represents the slope and friction source terms, respectively.

2.1.1. Flux terms

In order to update the flow variables to a new time level using Eq. (10), the interface fluxes ($\mathbf{F}_{i+1/2}^{n}$ and $\mathbf{F}_{i-1/2}^{n}$) must be properly evaluated and an HLL approximate Riemann solver (Harten et al., 1983; León et al., 2006; Sanders and Bradford, 2010) is adopted in this work:

$$\mathbf{F}=\begin{cases}\mathbf{F}_L & \text{if } S_L>0\\ \mathbf{F}^* & \text{if } S_L\le 0\le S_R\\ \mathbf{F}_R & \text{if } S_R<0\end{cases} \tag{11}$$

Table 1
The pipe-junction boundary calculation method.

	$h_J < d$	$h_J \geq d$
A_B	Eq. (4) and Eq. (5)	Calculate H_B first and then A_B using Eq. (9)
Q_B	$(u \times (\mathbf{n}_p \bullet \mathbf{n}_x) + v \times (\mathbf{n}_p \bullet \mathbf{n}_y)) \times A_B$	$(u \times (\mathbf{n}_p \bullet \mathbf{n}_x) + v \times (\mathbf{n}_p \bullet \mathbf{n}_y)) \times A_B$
H_B	0	Calculate I_B first and then H_B using Eq. (8)
I_B	Eq. (3)	Eq. (19)

in which $\mathbf{F}_L$ and $\mathbf{F}_R$ are numerical fluxes defined using the left and right Riemann states (i.e. the values of the flow variables reconstructed at the left and right cell interfaces, which are assumed to be the same as the cell-centre values for a first-order scheme), and $\mathbf{F}^*$ is calculated using the HLL flux formula:

$$\mathbf{F}^* = \frac{S_R\mathbf{F}_L - S_L\mathbf{F}_R + S_L S_R(\mathbf{U}_R - \mathbf{U}_L)}{S_R - S_L} \tag{12}$$

where S_L and S_R are the left and right characteristic wave speeds calculated by:

$$S_L = \min(V_L - c_L, V^* - c^*),\ S_R = \max(V^* + c^*, V_R + c_R) \tag{13}$$

in which V is the averaged flow velocity defined as $V = Q_p/A$ and V^* is calculated by:

$$V^* = \frac{1}{2}(V_L + V_R) + \frac{1}{2}(\phi_L - \phi_R) \tag{14}$$

where φ is a Riemann invariant relating to θ and its approximations are given by Sanders and Bradford (2010):

$$\phi_{L,R} \approx \beta\sqrt{\frac{gd}{8}}\sin\left(\frac{\theta_{L,R}}{4}\right), \beta = 6.41 \tag{15}$$

and subsequently

$$\phi^* = \frac{1}{2}(\phi_L + \phi_R) + \frac{1}{2}(V_L - V_R). \tag{16}$$

When $\phi^* \leq \beta\sqrt{gd/8}$, the flow is under free-surface condition and the intermediate wave speed c^* is calculated using

$$c^* = \sqrt{\frac{gd(\theta^* - \sin\theta^*)}{8\sin(\theta^*/2)}} \tag{17}$$

with

$$\theta^* = 4\arcsin\left(\frac{\phi^*}{\beta\sqrt{gd/8}}\right). \tag{18}$$

When $\phi^* > \beta\sqrt{gd/8}$, the water surface level may reach the crown of the pipe and the flow becomes pressurized. The intermediate wave speed c^* is then set to be the acoustic wave speed a for the pressurized interface flux computation.

When evaluating the fluxes at the interfaces between pipes and junctions, the boundary values of A_B, I_B, Q_B and H_B (with subtitle B representing 'boundary') must be obtained before the fluxes can be calculated using the approximate Riemann solver. The boundary variables can be calculated using the water depth h_J, velocities u and v at the x- and y-directions in the connected junction according to the following two cases:

(1) If $h_J < d$, the boundary cell is under a free-surface flow condition; A_B and I_B are calculated using Eq. (5) and Eq. (3), respectively. H_B does not exist in this case and Q_B will be obtained by projecting the flow rate in the junction along the normal direction of the pipe.

(2) If $h_J \geq d$, the pipe flow becomes pressurized. H_B is an unknown variable at the boundary interface, and hence I_B cannot be calculated using Eq. (8). A new approach is proposed herein to estimate the necessary boundary variables. Based on the hydrostatic pressure assumption, the pressure term I_B can be calculated using

$$I_B = g\left(h_J - \frac{1}{2}d\right)A_P \tag{19}$$

then H_B and A_B can be deduced from I_B and calculated using Eqs. (8) and (9), respectively. Q_B can be obtained in the same way as in case 1.

The detailed implementation of the pipe boundary calculation at a pipe-junction interface is summarised in Table 1, where $\mathbf{n}_p$ denotes the outward unit normal vector of the pipe interface; $\mathbf{n}_x$ and $\mathbf{n}_y$ are respectively the unit vector along the x- and y-directions in the local junction coordinate system.

2.1.2. Source terms

To update the flow variables using Eq. (10), it is also necessary to properly discretise the source terms. The bed slope terms are simply estimated using a central difference scheme and this will not create any numerical issues as the bed slopes of drainage pipes are commonly gentle and nearly horizontal in practice. For the friction source terms, an efficient fully implicit scheme originally developed for the 2D SWEs (Xia and Liang 2018) is adopted and modified herein for implementation in the current 1D TPA governing equations. Only the momentum equation in Eq. (10) contains a non-zero friction term and needs to be considered, which may be rewritten as

$$Q_{Pi}^{n+1} = Q_{Pi}^n - \Delta t\left(\frac{1}{\Delta x}\left[F_{i+1/2}^n - F_{i-1/2}^n\right] - S_{Pbi}^n\right) - \Delta t S_{Pfi}^{n+1} \tag{20}$$

where $S_{Pfi}^{n+1} = gn_P^2(P_i^n)^{\frac{4}{3}}Q_{Pi}^{n+1}|Q_{Pi}^{n+1}|/(A_i^n)^{\frac{7}{3}}$. Defining $\alpha = gn_P^2(P_i^n)^{\frac{4}{3}}/(A_i^n)^{\frac{7}{3}}$, Eq. (20) becomes:

$$\alpha\Delta t Q_{Pi}^{n+1}\left|Q_{Pi}^{n+1}\right| + Q_{Pi}^{n+1} - Q_{Pi}^n + \Delta t\left(\frac{1}{\Delta x}\left[F_{i+1/2}^n - F_{i-1/2}^n\right] - S_{Pbi}^n\right) = 0. \tag{21}$$

Further defining $B = -Q_{Pi}^n + \Delta t(\frac{1}{\Delta x}[F_{i+1/2}^n - F_{i-1/2}^n] - S_{Pbi}^n)$, the two sets of possible roots of the above quadratic equation are

$$Q_{Pi(1)}^{n+1} = \frac{-1 + \sqrt{1 - 4\alpha\Delta t B}}{2\alpha\Delta t} \quad \text{if } Q_{Pi}^{n+1} > 0 \tag{22}$$

$$Q_{Pi(2)}^{n+1} = \frac{-1 - \sqrt{1 - 4\alpha\Delta t B}}{2\alpha\Delta t} \quad \text{if } Q_{Pi}^{n+1} > 0 \tag{23}$$

and

$$Q_{Pi(3)}^{n+1} = \frac{-1 + \sqrt{1 + 4\alpha\Delta t B}}{-2\alpha\Delta t} \quad \text{if } Q_{Pi}^{n+1} < 0 \tag{24}$$

$$Q_{Pi(4)}^{n+1} = \frac{-1 - \sqrt{1 + 4\alpha\Delta t B}}{-2\alpha\Delta t} \quad \text{if } Q_{Pi}^{n+1} < 0. \tag{25}$$

Since $\alpha > 0$ is always true for any meaningful cases, both Eqs. (22) and (23) are negative if $B > 0$, which is not consistent with the condition of $Q_{Pi}^{n+1} > 0$. Also, Eq. (25) is positive when $B > 0$, which is not consistent with the condition of $Q_{Pi}^{n+1} < 0$. Therefore, Eq. (24) is the only admissible root for $B > 0$. Similarly, Eq. (22) is the only admissible root for $B < 0$. The two acceptable roots, Eqs. (22) and (24), can be then combined to provide a single analytical solution for Eq. (21), given as follows

$$Q_{Pi}^{n+1} = \frac{-1 + \sqrt{1 + 4\alpha\Delta t|B|}}{-2\alpha\Delta t\mathrm{Sgn}(B)} \tag{26}$$

where Sgn(•) denotes the sign function, i.e., $\mathrm{Sgn}(B)=\begin{cases}1 & \text{if } B>0\\ -1 & \text{if } B<0\end{cases}$. Substituting $\alpha=gn_P^2(P_i^n)^{\frac{4}{3}}/(A_i^n)^{\frac{7}{3}}$ in Eq. (26) leads to

$$Q_{Pi}^{n+1}=\frac{-1+\sqrt{1+4\Delta t|B|gn_P^2\left(P_i^n\right)^{\frac{4}{3}}\left(A_i^n\right)^{-\frac{7}{3}}}}{-2\Delta t\mathrm{Sgn}(B)n_P^2\left(P_i^n\right)^{\frac{4}{3}}\left(A_i^n\right)^{-\frac{7}{3}}} \tag{27}$$

where B can be easily obtained after solving the governing equations without friction terms using the adopted finite volume scheme.

If A_i^n is excessively small, $(A_i^n)^{-\frac{7}{3}}$ may create an extremely small value that exceeds the machine precision limit and hence cause numerical instability. To effectively avoid this, both the numerator and denominator of Eq. (27) are multiplied by $(A_i^n)^{\frac{7}{3}}$ and the final expression for Q_P^{n+1} is obtained

$$Q_{Pi}^{n+1}=\frac{-\left(A_i^n\right)^{\frac{7}{3}}+\sqrt{\left(A_i^n\right)^{\frac{14}{3}}+4\Delta t|B|gn_P^2\left(P_i^n\right)^{\frac{4}{3}}\left(A_i^n\right)^{\frac{7}{3}}}}{-2\Delta t\mathrm{Sgn}(B)n_P^2\left(P_i^n\right)^{\frac{4}{3}}}. \tag{28}$$

2.2. Junction model

Free-surface flow conditions commonly apply when calculating junction flows even when the water depth in the junction submerges all of the connecting pipes and the pipe flows are pressurized. In this work, each of the junctions in a drainage system is idealized as a 2D domain and the flow is subsequently calculated using a model that solves the fully 2D SWEs to (1) automatically take into account mass and momentum conservation, and (2) avoid setting complicated BCs for calculating pipe flows. For example, Fig. 1 illustrates a schematic diagram for a junction connecting three pipes. The diameter of each pipe is denoted by d_i ($i=1, 2, 3$); P1 and P2 are assumed to be inflow pipes while P3 is an outflow pipe. Based on the layout of the inflow and outflow pipes, the junction domain is approximated using an irregular 2D grid cell as shown in Fig. 1(b). On such a grid, a cell-centred finite volume scheme is implemented to solve the 2D SWEs to predict the flow dynamics in the junction. In this case, the inflows from the two incoming pipes (P1 and P2) are mixed and then discharged into the outflow pipe (P3). During a simulation, the cell edges connecting the pipes are all defined as 'open' boundaries, through which the inflow and outflow discharges (q_1, q_2 and q_3) from the connecting pipes are obtained from the pipe calculations and imposed as the boundary conditions for the 2D junction flow calculation. The inflow and outflow pipes are automatically defined according to the flow directions predicted by the pipe model. This essentially defines a two-way dynamic coupling scheme that links seamlessly the junction model with the pipe model, effectively avoiding the requirement of any complicated BCs for the pipe flow calculations.

The 2D SWEs describing the free-surface flow in a junction may be written in a matrix form as

$$\frac{\partial\mathbf{U}_J}{\partial t}+\frac{\partial\mathbf{F}_J}{\partial x}+\frac{\partial\mathbf{G}_J}{\partial y}=\mathbf{R}+\mathbf{S}_{Jb}+\mathbf{S}_{Jf} \tag{29}$$

where the vector terms are given by

$$\mathbf{U}_J=\begin{bmatrix}h_J\\ uh_J\\ vh_J\end{bmatrix},\ \mathbf{F}_J=\begin{bmatrix}uh_J\\ u^2h_J+\frac{1}{2}gh_J^2\\ uvh_J\end{bmatrix},\ \mathbf{G}_J=\begin{bmatrix}vh_J\\ uvh_J\\ v^2h_J+\frac{1}{2}gh_J^2\end{bmatrix}$$
$$\mathbf{R}=\begin{bmatrix}R\\ 0\\ 0\end{bmatrix},\ \mathbf{S}_{Jb}=\begin{bmatrix}0\\ -gh_J\frac{\partial z_b}{\partial x}\\ -gh_J\frac{\partial z_b}{\partial y}\end{bmatrix}\text{ and }\mathbf{S}_{Jf}=\begin{bmatrix}0\\ -\frac{\tau_{bx}}{\rho}\\ -\frac{\tau_{by}}{\rho}\end{bmatrix} \tag{30}$$

where the subscript J represents the junction; u and v are the depth-averaged velocities along the x- and y-directions, respectively; $\mathbf{F}_J$ and $\mathbf{G}_J$ are the flux terms; $\mathbf{R}$, $\mathbf{S}_{Jb}$ and $\mathbf{S}_{Jf}$ contain respectively the mass, slope and friction source terms; R is the external unit flow rate; τ_{bx} and τ_{by} are bed friction stresses calculated by $\tau_{bx}=\rho C_f u\sqrt{u^2+v^2}$ and $\tau_{by}=\rho C_f v\sqrt{u^2+v^2}$, with $C_f=gn_J^2/h_J^{1/3}$ being the bed roughness coefficient and n_J being the Manning coefficient at the junction.

When implementing the above junction model, a finite volume scheme is employed and the resulting time-marching formula is written as

$$\mathbf{U}_J^{n+1}=\mathbf{U}_J^n-\frac{\Delta t}{\Omega}\mathbf{P}+\Delta t\left(\mathbf{R}^n+\mathbf{S}_{Jb}^n+\mathbf{S}_{Jf}^{n+1}\right). \tag{31}$$

To couple with the 1D pipe model, the flux terms $\mathbf{F}_J$ and $\mathbf{G}_J$ in the Eq. (30) has been revised and the new flux term is denoted as $\mathbf{P}$ (see Section 2.2.1). Ω is the cell area that is set to be the actual junction area, and hence its value is independent of the cell configuration.

2.2.1. Evaluating the flux terms

As illustrated in Fig. 1, two different fluxes inside a junction cell are considered: (1) the flux across the interface between junction and the connecting pipes, denoted by $\mathbf{P}_{pk}$ for the kth pipe; and (2) a no-flow flux at the wall interface, denoted by $\mathbf{P}_w$. Therefore, the flux vector can be written as

$$\mathbf{P}=\sum_{k=1}^{N}\mathbf{P}_{pk}+\mathbf{P}_w \tag{32}$$

where N is the number of the pipes connected to the junction.

(1) Fluxes through a pipe-junction interface

To ensure strict mass and momentum conservation between the 1D pipe model and the 2D junction model, the fluxes obtained from the 1D TPA calculation are converted into the local junction coordinate system to derive the numerical fluxes through the corresponding cell interfaces:

$$\mathbf{P}_{pk}=\begin{bmatrix}1 & 0\\ 0 & \mathbf{n}_{pk}\cdot\mathbf{n}_x\\ 0 & \mathbf{n}_{pk}\cdot\mathbf{n}_y\end{bmatrix}\cdot\begin{bmatrix}F_{1k}\\ F_{2k}\end{bmatrix} \tag{33}$$

where $\mathbf{n}_{pk}$ denotes the outward unit normal vector of the *k-th* pipe interface, $\mathbf{F}=[F_{1k}\ \ F_{2k}]^T$ contains the mass and momentum fluxes of 'Pipe k' predicted by the 1D TPA model.

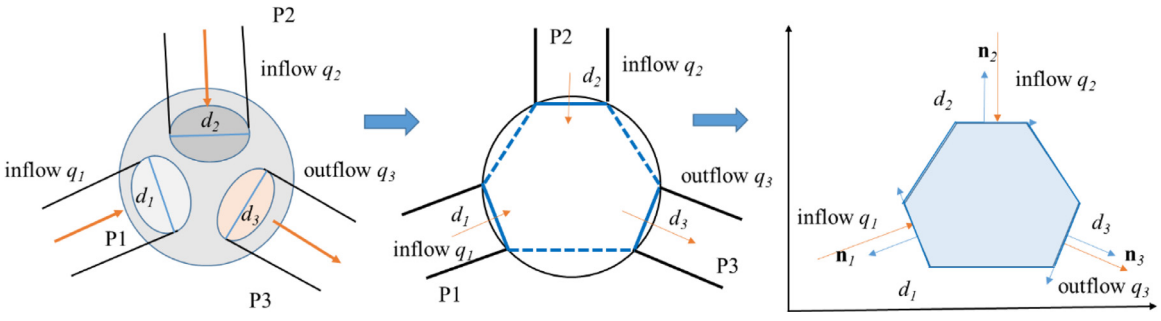

Fig. 1. Spatial discretization scheme for a junction.

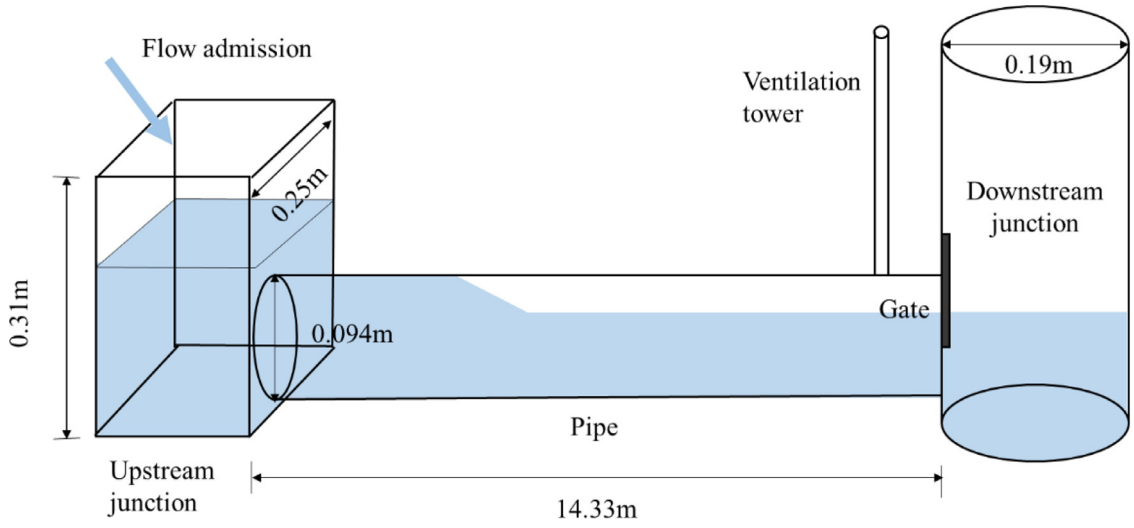

Fig. 2. Experimental pressurised flow test: experimental apparatus and set up.

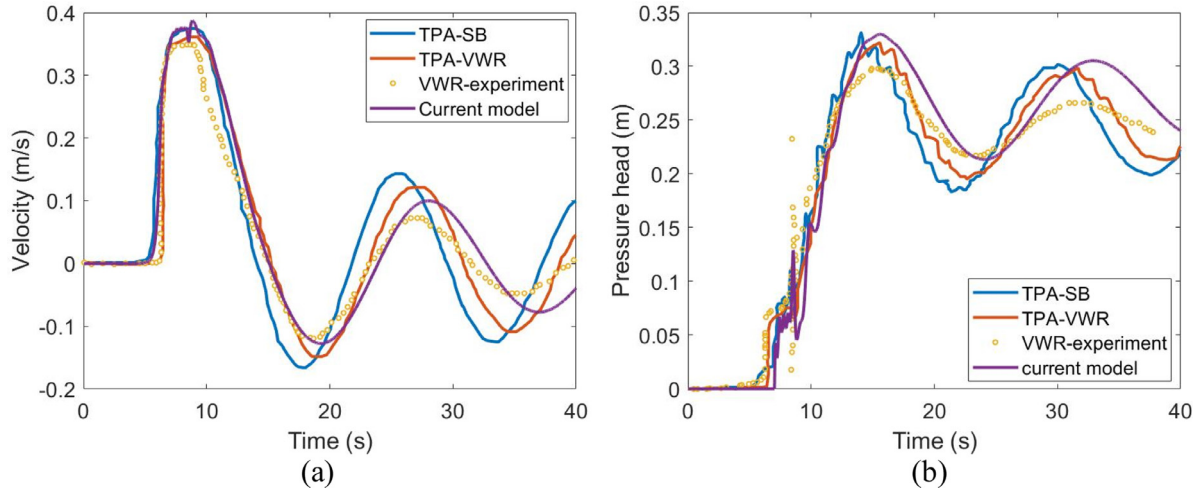

Fig. 3. Flow variables at $x = 9.9$ m predicted by the new drainage model, TPA-SB model and TPA-VWR model, in comparison with the VWR experimental measurements: (a) velocity; (b) pressure. (For interpretation of the references to color in this figure, the reader is referred to the web version of this article.)

(2) Fluxes at a wall interface

At the junction interface that is not connected to a pipe, it is effectively a wall boundary and no flow is allowed to cross the interface. Subsequently, only the pressure terms in the momentum equations are effective for the flux calculation. A novel approach is proposed and used to evaluate the pressure terms in this work. A junction connecting to three pipes as illustrated in Fig. 1 is again used as a demonstrative example. Considering the fluid/water inside this enclosed domain (i.e. the junction), the final net hydrostatic pressure adding on the entire enclosed fluid boundary must be physically integrated to zero. Subsequently considering a force balance, the total hydrostatic force acting on all of the interfaces between the pipes and the junction must be equal to that imposed on the interface between the surrounding wall (excluding the pipe areas) and the fluid, but in the opposite direction. The net pressure forces on the pipe-junction interfaces may be then used to deduce the hydrostatic force adding on the wall interface so that the fluxes can subsequently be derived and given by

$$\mathbf{P}_w = -\begin{bmatrix} 0 \\ \sum_{k=1}^{N} \mathbf{n}_{pk} \cdot \mathbf{n}_x \cdot I_{pk} \\ \sum_{k=1}^{N} \mathbf{n}_{pk} \cdot \mathbf{n}_y \cdot I_{pk} \end{bmatrix} \tag{34}$$

where I_{pk} denotes the pressure flux at the interface between the *k-th* pipe and the junction. When the junction water depth h_J is smaller than the pipe diameter, the pipe flow is under free-surface conditions and I_{pk} can be calculated according to Eq. (3); when h_J rises higher than the crown level of the pipe, pressurised flow occurs, and I_{pk} should be computed according to Eq. (19).

2.2.2. Source terms

For the source terms in Eq. (31), the mass term R (e.g. rainfall rate) will be calculated or prescribed. The slope terms are set to be zero since each of the junctions is approximated as a single cell and the bed elevation is considered to be homogeneous inside the cell. The fully implicit friction discretization scheme proposed by Xia and Liang (2018) is implemented to discretise the friction source terms to ensure stable simulation when the water depth becomes small.

2.3. Stability criteria

Since the finite volume schemes adopted for the 1D pipe model and 2D junction model are both overall explicit, the time step for the final coupled drainage network model is controlled by the CFL condition defined as follows:

$$\Delta t = \mathrm{CFL} \times \min(\Delta t_P, \Delta t_J) \tag{35}$$

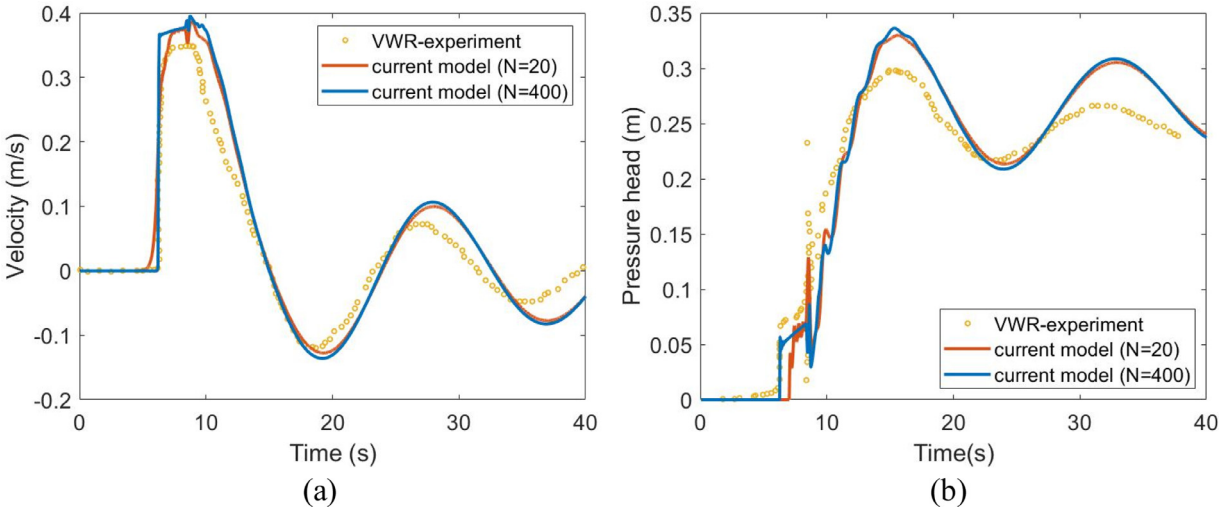

Fig. 4. Flow variables at $x = 9.9$ m predicted at different grid resolutions: (a) velocity; (b) pressure.

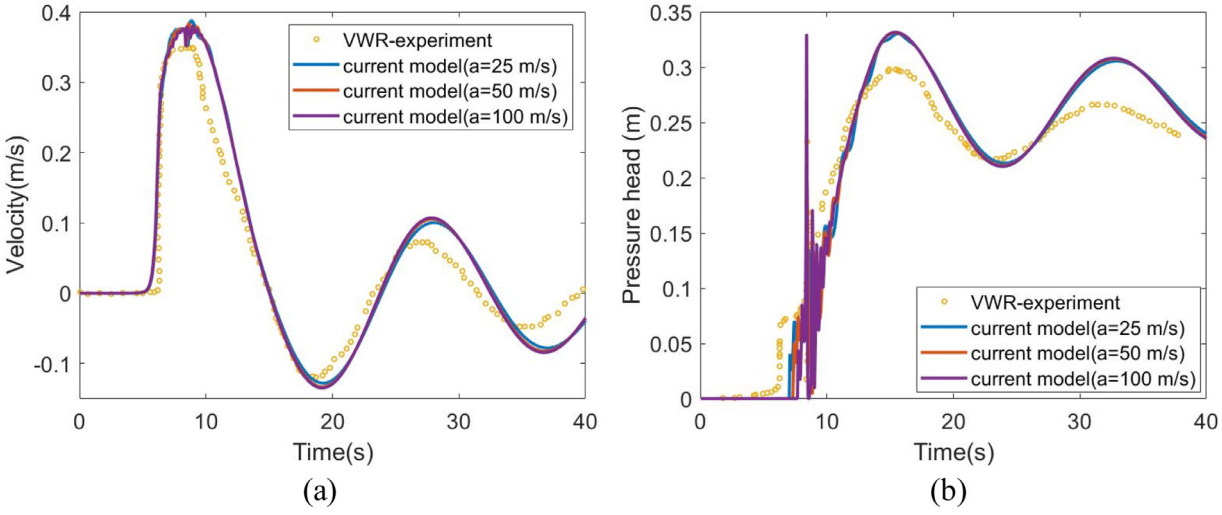

Fig. 5. Flow variables at $x = 9.9$ m predicted using different wave speeds: (a) velocity; (b) pressure.

where the CFL number is generally $0 < \text{CFL} \leq 1$ and is set to be 0.5 for all of the simulations considered in this work; Δt_P and Δt_J are defined as:

$$\Delta t_P = \begin{cases} \min\left(\frac{dx}{(|Q_{Pi}|/A_i + a)}\right) & \text{if } A_i^n > A_P \\ \min\left(\frac{dx}{(|Q_{Pi}|/A_i + c_i)}\right) & \text{if } A_i^n \leq A_P \end{cases},$$

$$\Delta t_J = \min\left(\frac{\sqrt{\Omega_i}}{\sqrt{\left((u)_{Ji}\right)^2 + \left((v)_{Ji}\right)^2} + \sqrt{g h_J}}\right) \tag{36}$$

3. Results and discussion

In this section, one experimental and three idealized test cases are simulated to validate the new drainage model and demonstrate its performance for pipe network simulations.

3.1. Experimental test

In order to validate the proposed drainage model for the accurate simulation of transitional flow inside a drainage system, an experimental test case is considered in this section and the numerical results are compared with the laboratory measurements reported by Vasconcelos et al. (2006) (VWR experiment), and also the alternative numerical predictions from the TPA model presented by Vasconcelos et al. (2006) (TPA-VWR) and another TPA sewer network model proposed by Sanders and Bradford (2010) (TPA-SB).

Fig. 2 illustrates the laboratory apparatus, which consists of an acrylic horizontal pipe connected by two junctions at both ends. The pipe is 14.33 m in length and 9.4 cm in diameter. The upstream junction has a square base of 25 cm side length. The downstream cylindrical tank is 19 cm in diameter and is supposed to be deep enough to prevent overflowing. A gate is installed at the downstream end of the pipe to prevent air from entering the cylindrical junction when the pipe is flooded. A ventilation tower located just upstream of the gate is also installed to expel air from the pipe when it is under a pressurized condition. During the simulation, the wave speed a is set to 25 m/s and the Manning coefficient is 0.012 $\text{m}^{-1/3}$ s. The pipe is discretized using 20 cells to give $\Delta x = 0.7165$m. The simulation begins with an initial water at rest throughout the whole system. The still free-surface water depth at the junctions is 7.3 cm above the pipe invert. A 3.1 l/s flow is imposed at the upstream junction to create a transient flow into the pipe, which is regulated by a weir overflow structure integrated into the model as suggested by Sanders and Bradford (2010).

Fig. 3(a) shows the flow velocities at $x = 9.9$ m (from the left-hand-side edge of the pipe), in which the numerical predictions from

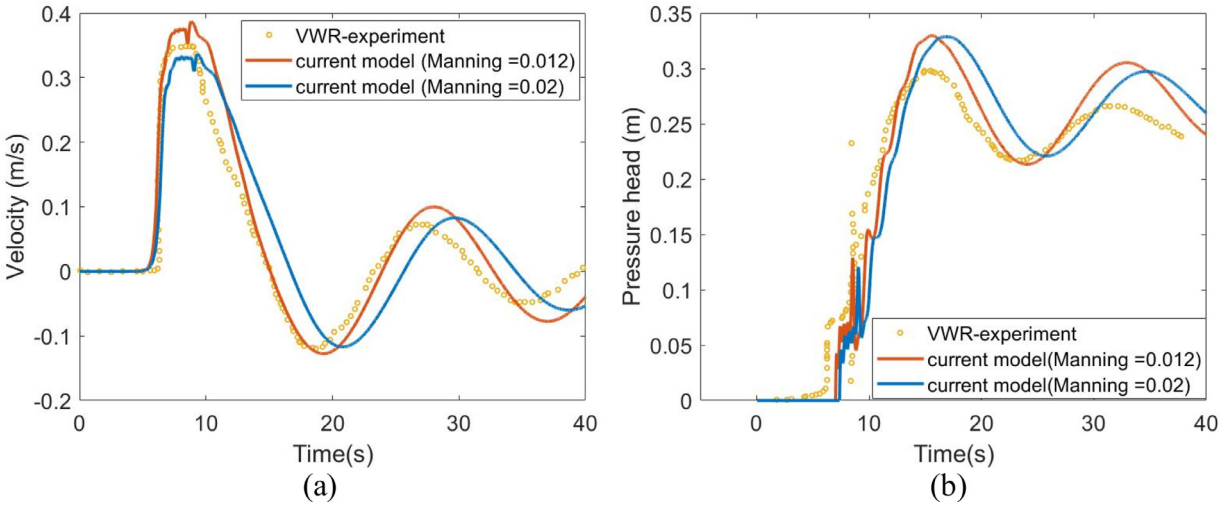

Fig. 6. Flow variables at $x = 9.9$ m predicted using different Manning coefficients: (a) velocity; (b) pressure.

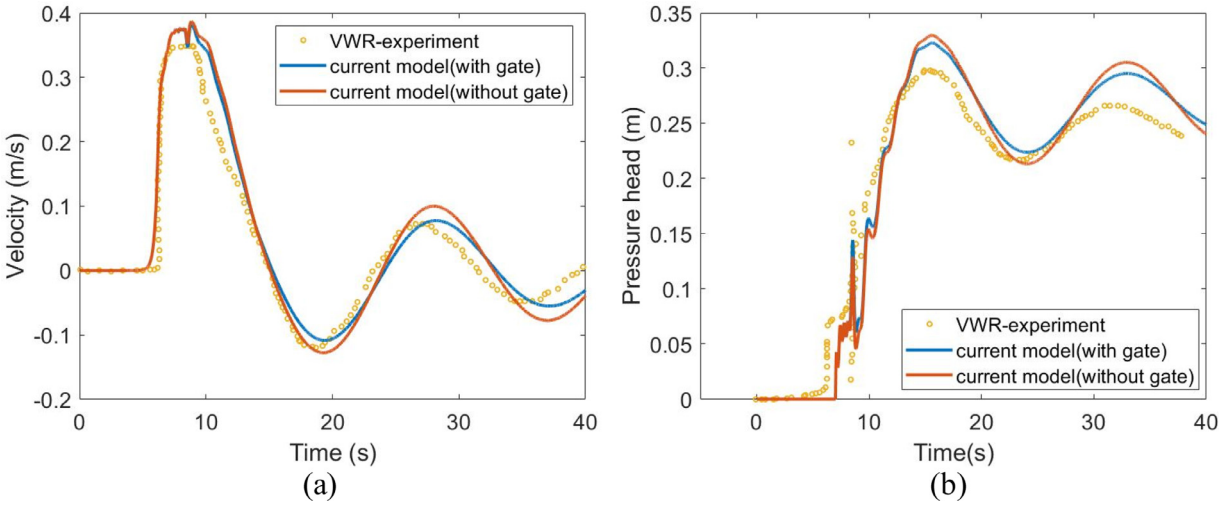

Fig. 7. Flow variables at $x = 9.9$ m predicted with/without a gate: (a) velocity; (b) pressure.

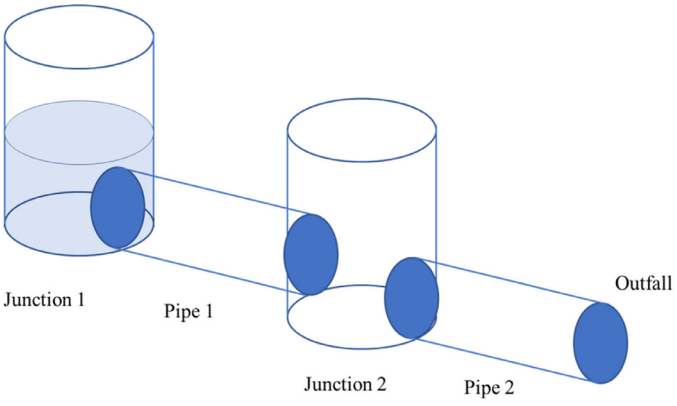

Fig. 8. Configuration of the idealized drainage system.

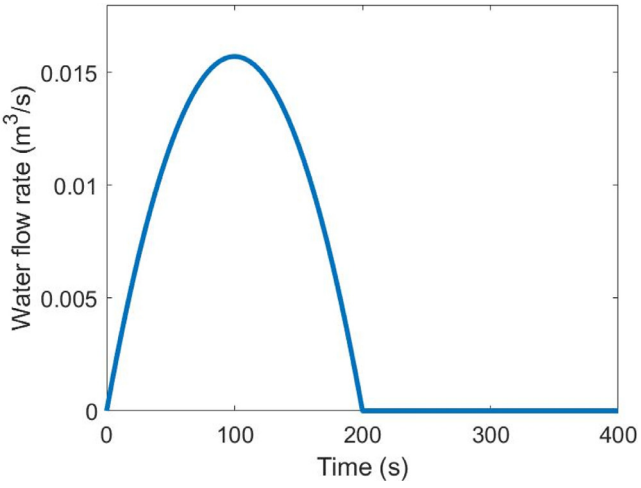

Fig. 9. The external flow rate imposed at Junction 1.

the current drainage model (purple line), the TPA-VWR model (red line) and the TPA-SB model (blue line) are compared with the experimental measurements (yellow circle). It is shown that the current model satisfactorily reproduces the time history of the velocity including peak values and the results are consistent with the two alternative models (i.e. TPA-SB and TPA-VWR). Fig. 3(b) compares the pressure simulated by the three models with measurements at the same cross-section. All three models produce results that are again consistent with the experiment measurements although the predictions of pressure surges are slightly overestimated.

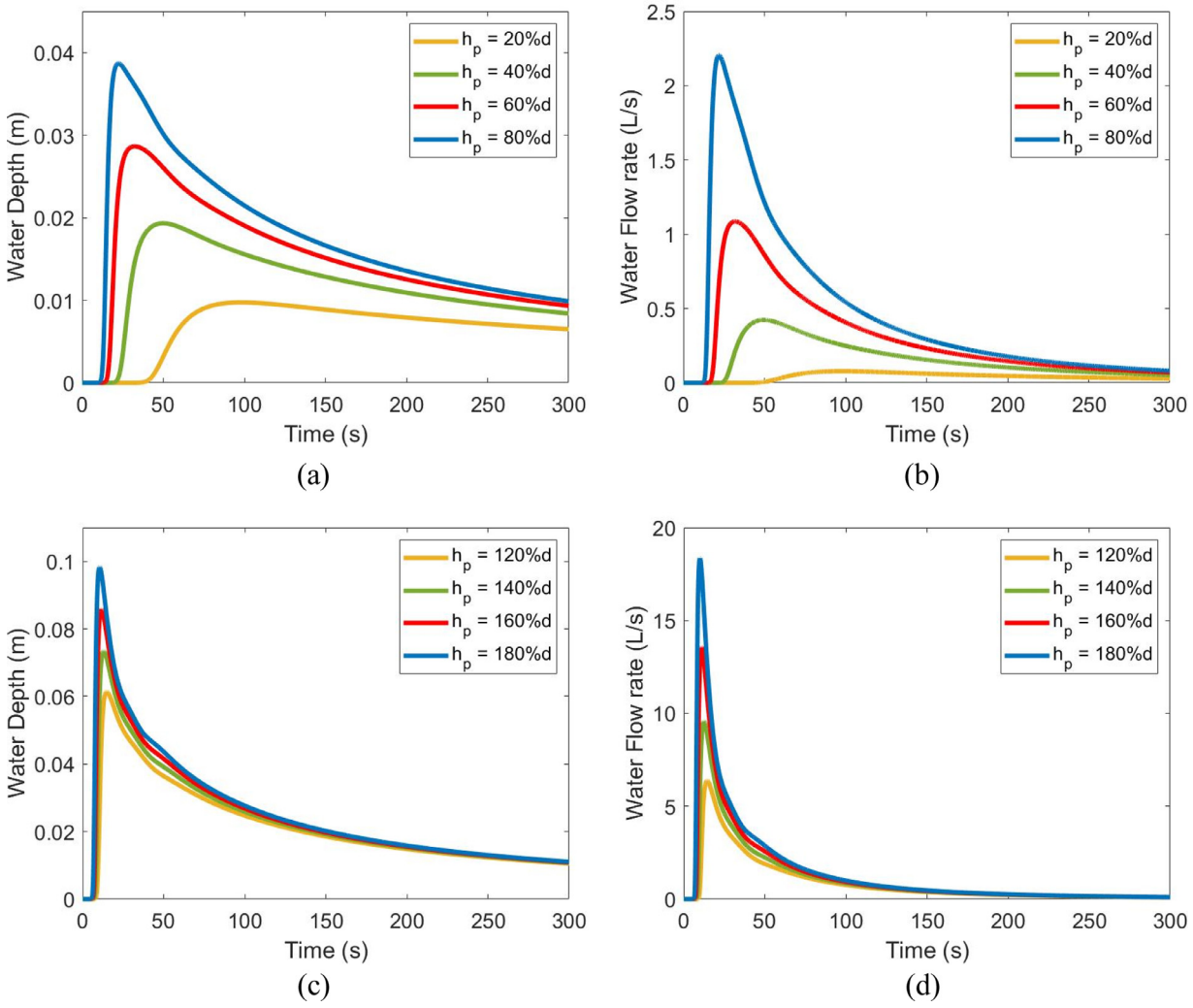

Fig. 10. Predicted water depths and flow rates at the outfall for Case 1: (a) water depths under a free surface flow condition; (b) flow rates under a free surface flow condition; (c) water depths under a pressurized flow condition; (d) flow rates under a pressurized flow condition; 'h_p' denotes the initial water depth in Junction 1 and 'd' refers to the pipe diameter.

Further simulations are carried out to investigate the sensitivity of the simulation results to relevant model parameters. Fig. 4 shows the predictions of flow velocity and pressure at the same location using different grid resolutions to discretize the pipe, i.e. $N = 20$ and $N = 400$, respectively, where other model parameters remain the same. The simulation results produced at high and low resolutions are in close agreement for both flow velocity and pressure. Fig. 5 presents the results obtained using different acoustic wave speeds (i.e., $a = 25$, 50 and 100 m/s). The predicted velocities are consistent and close to each other for all of the three selected acoustic wave speeds. However, the pressure produced with $a = 100$ m/s presents post-shock oscillations of large magnitude at around $t = 8$ s. Post-shock oscillations are commonly observed in the simulations involving mixed flow regimes using TPA or Pressman slot models due to the existence of a discontinuity in the wave speed. For the current case, it is recommended to use $a = 25$ m/s to reduce the numerical oscillations in the solution. Fig. 6 provides further simulation results obtained using two different Manning coefficients, i.e. $0.012\,\mathrm{m}^{-1/3}$ s and $0.02\,\mathrm{m}^{-1/3}$ s. The results show a certain level of sensitivity to the Manning coefficient. When increasing the Manning coefficient from $0.012\,\mathrm{m}^{-1/3}$ s to $0.02\,\mathrm{m}^{-1/3}$ s, the peak velocity slightly reduces and there is a small shift change in the temporal profile of the velocity (Fig. 6(a)), which is accordingly reflected in the pressure profile as shown in Fig. 6(b). Finally, the effect induced by the gate installed at the downstream end of the pipe is also investigated, and the results are presented in Fig. 7. This partially closed gate may influence the flow hydrodynamics and Sanders and Bradford (2010) suggested to add a local head loss term to take into account the effect (with the head loss coefficient set to be 1.25). After incorporating the gate effect, the model produces results that are compared slightly better with the experimental measurements.

3.2. *Unsteady flow through different drainage settings*

This idealized test is designed to demonstrate the effect of different junction-pipe settings on the simulation results. Fig. 8 illustrates a simple drainage system with two horizontal pipes connecting to two junctions with a radius of 0.5 m and one outfall. Water inside Junction 1 will flow through the pipe to Junction 2 and then discharge through the outfall at the end of Pipe 2. During the simulations, the Manning coefficient in the whole junction-pipe domain is set to be $0.035\,\mathrm{m}^{-1/3}$ s. The pipes are discretized using uniform grids at 0.5 m resolution. Three cases are considered:

Case 1: Both of the pipes are 6 m long with a diameter of 0.5 m. The upstream Junction 1 is initialised with different water depths (i.e. 20%, 40%, 60% and 80% of the pipe diameter for free surface flow, and 120%, 140%, 160% and 180% of the pipe diameter for transitional pressurized flow) to generate different unsteady flows.

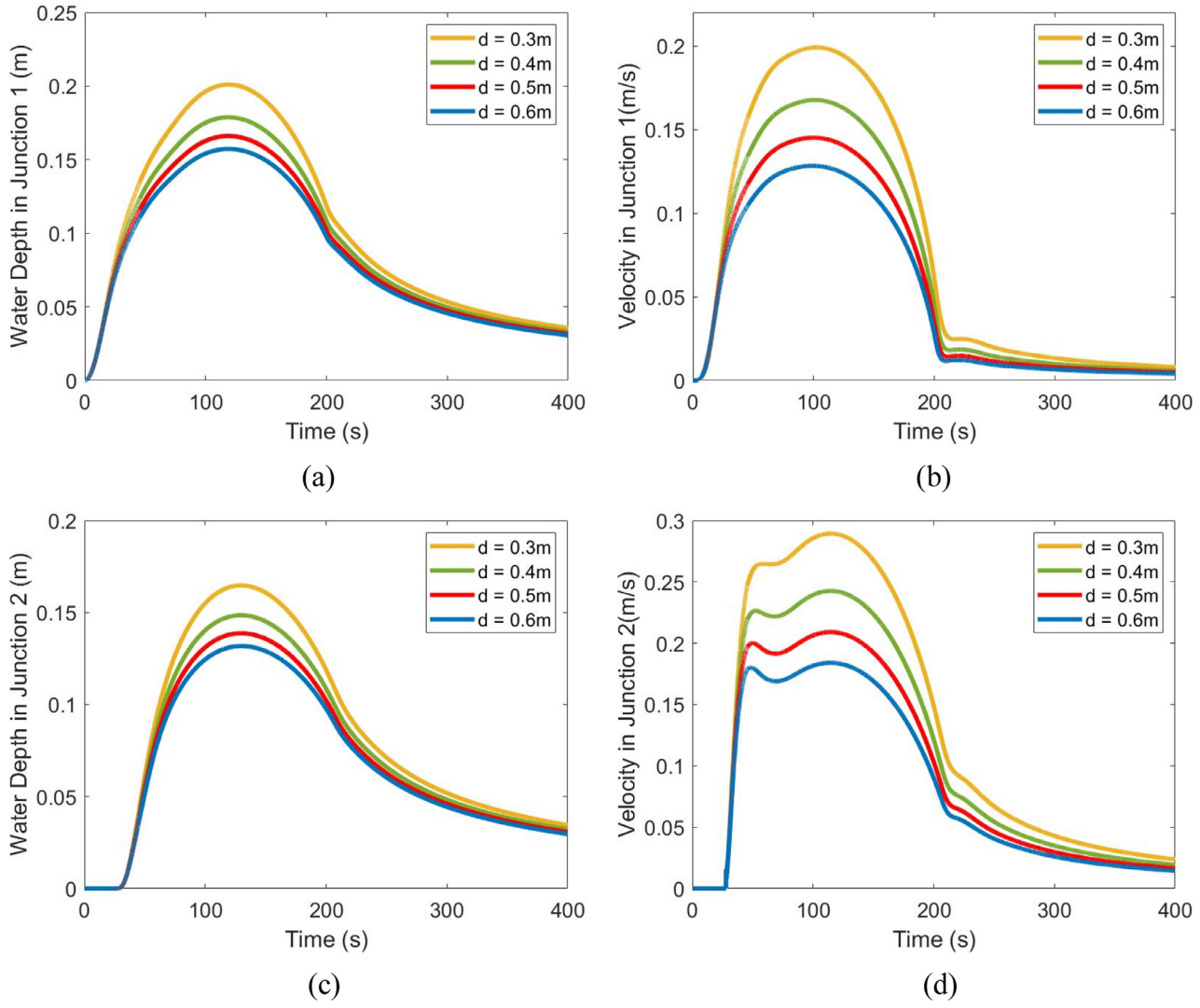

Fig. 11. Predicted water depths and velocities in the two junctions for Case 2: (a) water depth at Junction 1; (b) flow velocity at Junction 1; (c) water depth at Junction 2; (d) flow velocity at Junction 2.

Case 2: The length of the pipes remains to be 6 m but different pipe diameters are used (i.e. 0.3, 0.4, 0.5 and 0.6 m) to investigate the response of the junction flow to the change of size ratio between the pipes and junctions. The whole system is dry initially and an external inflow as given in Fig 9 is imposed at Junction 1. All of the simulations last for 400 s.

Case 3: Different pipe lengths (i.e. 3 m, 6 m and 12 m) are further used to explore the effect of pipe length on junction flows. The pipe diameter is fixed at 0.5 m. Initial and inflow conditions are set to be the same as Case 2.

For Case 1, Fig. 10(a) and (b) presents the time histories of free-surface water depth and flow rate at the outfall predicted for different initial depths in Junction 1. With the increase of the initial water depth, the model predicts higher peaks of both the water depth and flow rate. Fig. 10(c) and (d) shows the temporal change of water depth and flow rate at the outfall under a pressurized flow condition. It is evident that the predicted peaks of both water depth and flow rate under a pressurized condition are much sharper than those produced under a free-surface condition for all of the simulations involving different initial depths. All of the simulation results are as expected since the higher head at the upstream Junction 1 drives the flow with higher velocity along this simple and straight junction-pipe system, and the pressure in the upstream junction aggravates this driving force.

Fig. 11 shows the simulation results in terms of flow depth and velocity in the two junctions for Case 2, where the pipe diameter varies between 0.3 m and 0.6 m. Fig. 11(a) presents the time histories of water depth in Junction 1. It is observed that higher water depth in Junction 1 is predicted for smaller pipe diameters, which is as expected due to the lower discharge capacity for smaller pipes. Fig. 11(b) plots the temporal change of flow velocities in Junction 1. The peak velocity decreases as pipe diameter increases, which is consistent with the water depth predictions as shown in Fig. 11(a). Fig. 11(c) and (d) illustrates the predicted water depths and velocities in the Junction 2. In both junctions, the water depth shows the similar shape as the external flow. Compared with the results in Junction 1, the peak values of the water depth decrease while the peak velocities increase for the same pipe diameter, which is again as expected. Intuitively, a smaller pipe diameter will lead to lower drainage capacity and higher water depth in Junction 1. The higher water depth in turn provides a larger head difference to drive an unsteady flow with higher momentum in the downstream connecting pipe (Pipe 1) and junction (Junction 2).

Fig. 12 shows the simulation results for Case 3 where the pipe length changes between 3 m and 12 m. Fig. 12(a) and (b) respectively plots the predicted water depths and flow velocities in Junction 1. The peak water depth in Junction 1 increases (Fig. 12(a)) as the pipes become longer but the corresponding peak velocity decreases (Fig. 12(b)). The

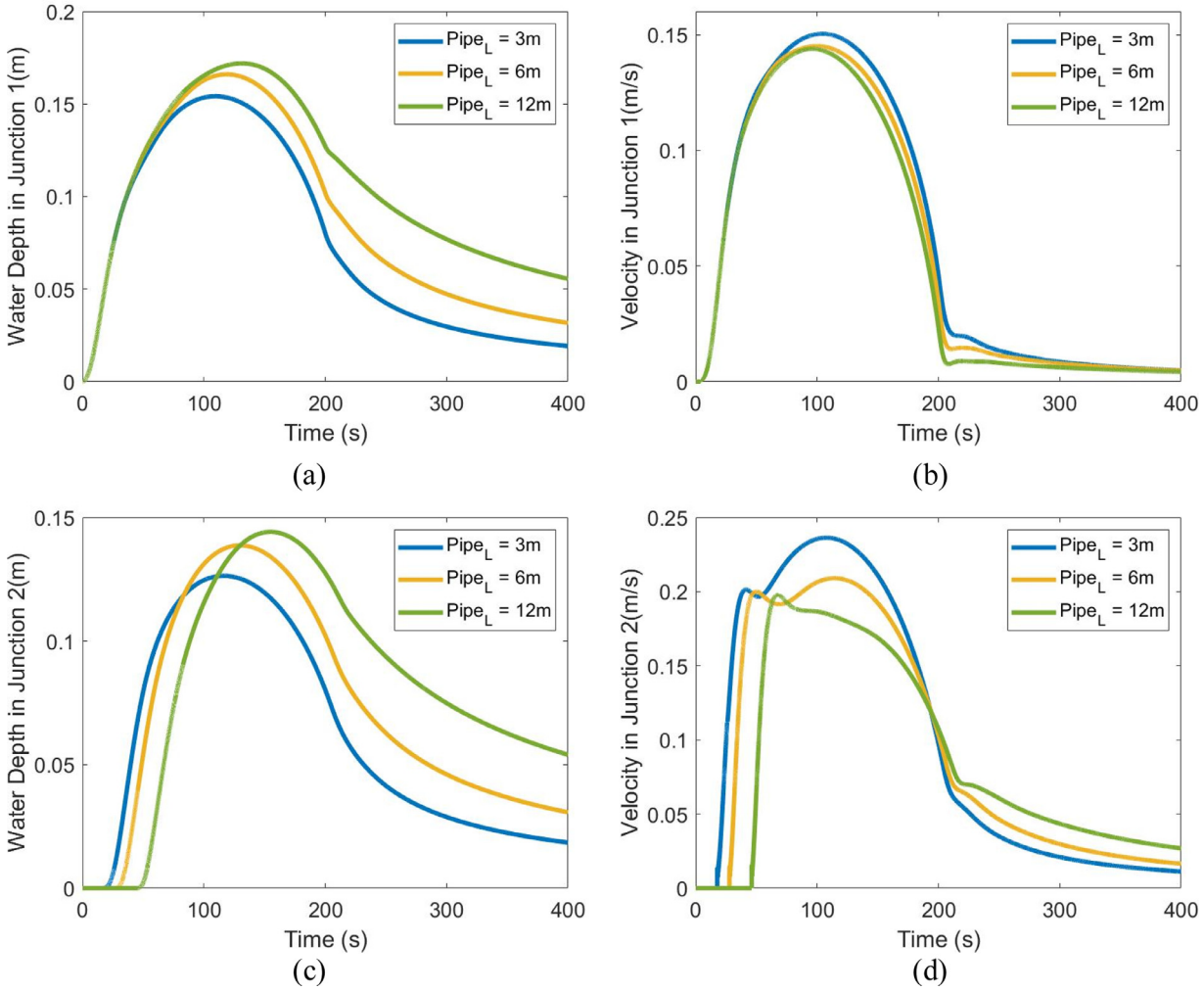

Fig. 12. Predicted water depths and velocities in the two junctions for Case 3: (a) water depth at Junction 1; (b) flow velocity at Junction 1; (c) water depth at Junction 2; (d) flow velocity at Junction 2; 'Pipe$_L$' denotes pipe length.

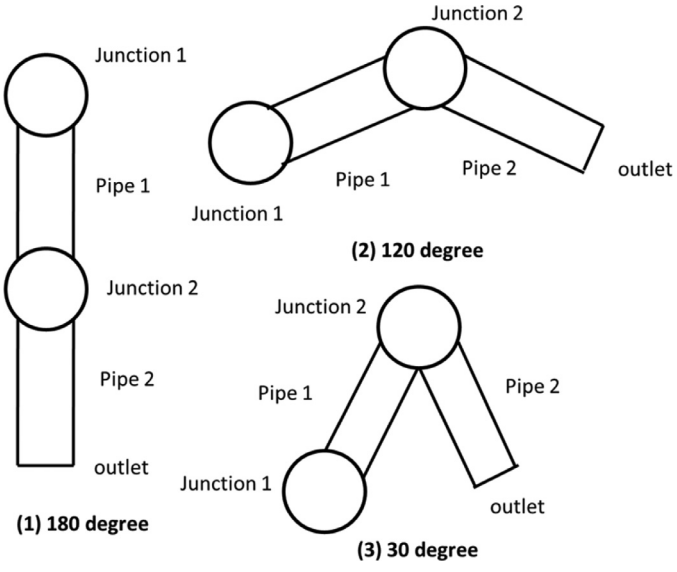

Fig. 13. V-shape networks of three different connecting angles: 180^0, 120^0 and 30^0.

simulation results in Junction 2, as presented in Fig. 12(c) and (d), are consistent with the results in Junction 1. As the pipe becomes longer, it takes longer for the flow to reach Junction 2 and the predicted flow velocity in Junction 2 appears to be more sensitive to the pipe length (Fig. 12(d)). Since the drainage system is horizontal, the flow is only affected by the head difference and friction; driven by the same external flow, the longer pipes induce more friction losses and dissipate more momentum, which subsequently slows down the flow and causes the water depths inside both junctions to rise and flow velocities to decrease. Overall, all of the simulation results follow the physical processes of the water flow, demonstrating the capacity of the current model in predicting unsteady flows in a simple junction-pipe system.

3.3. Unsteady flow in V-shape networks

Three V-shape networks with different connecting angles are designed to investigate the importance of considering momentum exchange in the junction flow calculations. As illustrated in Fig. 13, two pipes are connected to a common junction at three different angles, i.e. 180^0, 120^0 and 30^0. Both of the pipes are 10 m long and 2.07 m in diameter and both of the two junctions have a radius of 4 m. During the simulations, the Manning coefficient of the whole system is set to $0.035\,\mathrm{m}^{-1/3}\,\mathrm{s}$. The pipes are discretized using a uniform grid of 0.5 m

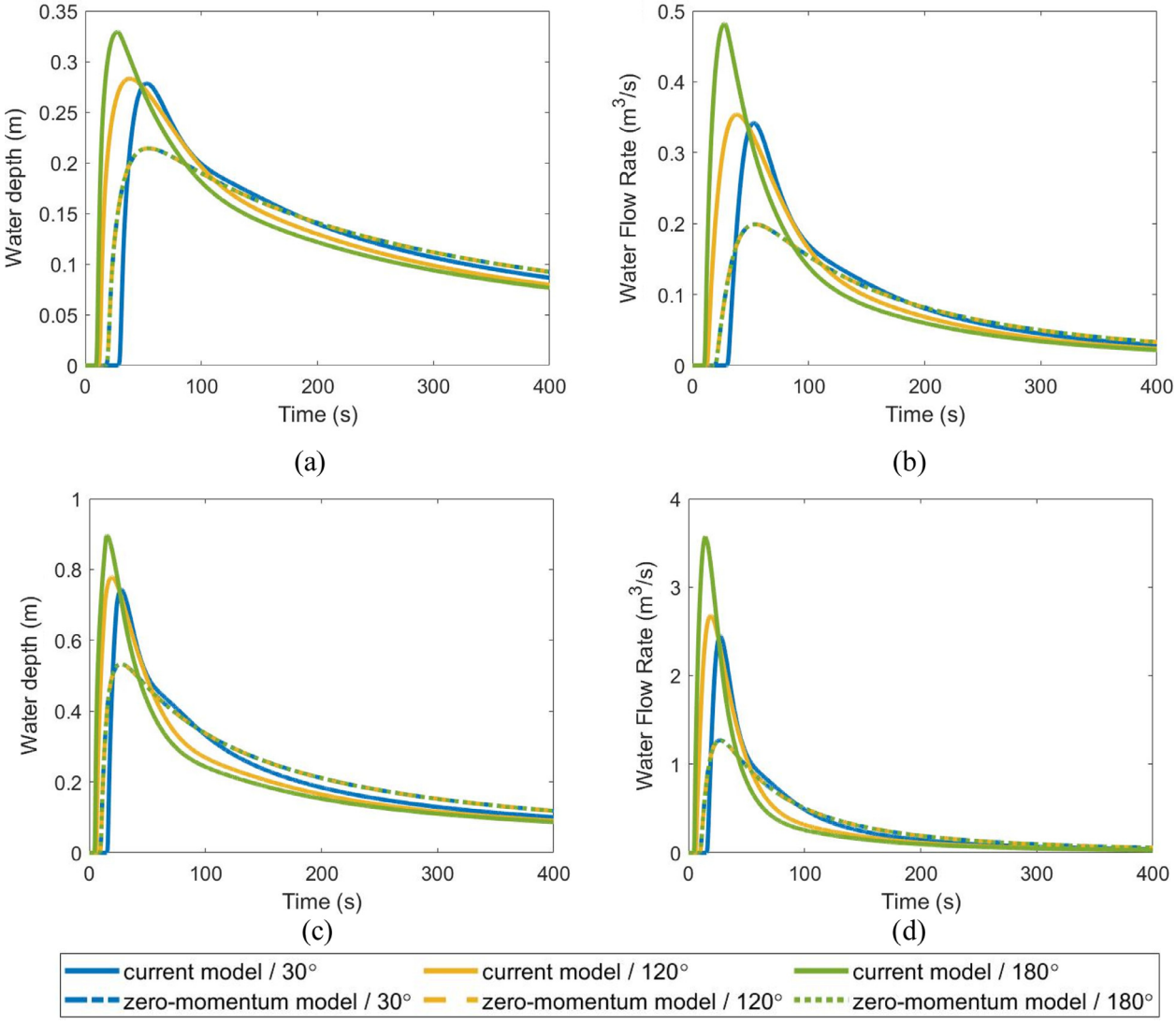

Fig. 14. Predicted water depths and flow rates at the outfalls of the three V-shape junction-pipe systems: (a) water depths under a free surface flow condition; (b) flow rates under a free surface flow condition; (c) water depths under a pressurized flow condition; (d) flow rates under a pressurized flow condition.

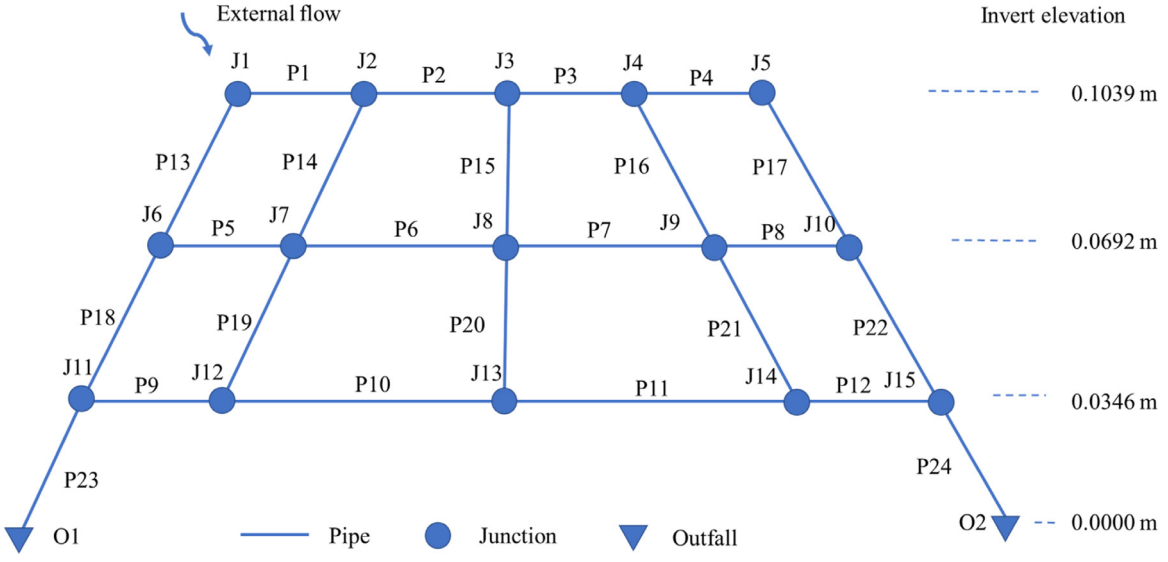

Fig. 15. The configuration of a hypothetical drainage network.

Table 2
Pipe length (m).

Index	Length	Index	Length	Index	Length	Index	Length	Index	Length
1	10	2	10	3	10	4	10	5	10
6	20	7	20	8	10	9	10	10	30
11	30	12	10	13	20	14	20	15	17.32
16	20	17	20	18	20	19	20	20	17.32
21	20	22	20	23	20	24	20		

Table 3
Junction radius (m).

Index	Radius	Index	Radius	Index	Radius	Index	Radius	Index	Radius
1	0.5	2	0.6	3	0.6	4	0.6	5	0.5
6	0.6	7	0.75	8	0.75	9	0.75	10	0.6
11	0.6	12	0.75	13	0.75	14	0.75	15	0.6

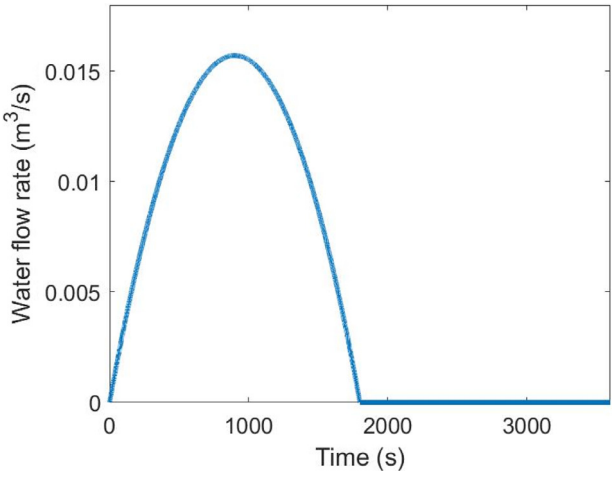

Fig. 16. External inflow hydrograph imposing at Junction 1.

resolution. Initially, the still water depth in Junction 1 is set to 1.24 m (60% of the pipe diameter) for the free-surface flow simulations and to 3.31 m (160% of the pipe diameter) for the transitional pressurized flow simulations, respectively. To quantify the effect of momentum exchange in junction flow calculation, the predictions with the flow velocity inside the junctions set to zero (i.e. neglecting momentum exchange; named "zero-momentum model" herein) are compared with the simulation results predicted by the current model with momentum conservation automatically taken into account by the 2D SWE model.

Fig. 14 compares the water depths and flow rates predicted by the models with and without taking into account momentum exchange in the junctions for the V-shape junction-pipe systems with different connecting angles. For both of the free surface and pressurized flows, it is clear that the difference between the peak flow values (i.e. peak water depth and peak flow rate) predicted by the models with and without considering momentum transfer becomes more predominant as the connecting angle increases. This is because an acute connecting angle would cause more energy loss inside the junction, leading to a lower flow velocity/momentum into the discharging pipe. When the connecting angle reaches 180^0, the momentum of the flow from the upstream Pipe 1 will be completely transferred to the middle junction and then to Pipe 2. The effect of varying the connecting angle is evidently captured in the results produced by the current drainage model. However, the results obtained from the model with a zero junction velocity show no differences when the connecting angle is changed, which is clearly not in line with practice. This may become particularly problematic for the simulation of intense rainfall induced flood events in which the flood hydrodynamics in the drainage networks may be highly transient and can only be reliably predicted when momentum exchange in junctions is properly taken into account. Therefore, it is essential to consider momentum conservation in junction flow calculation to ensure reliable simulation results. This test case effectively confirms this and demonstrates that the current drainage model can automatically reinforce momentum conservation in junction calculation.

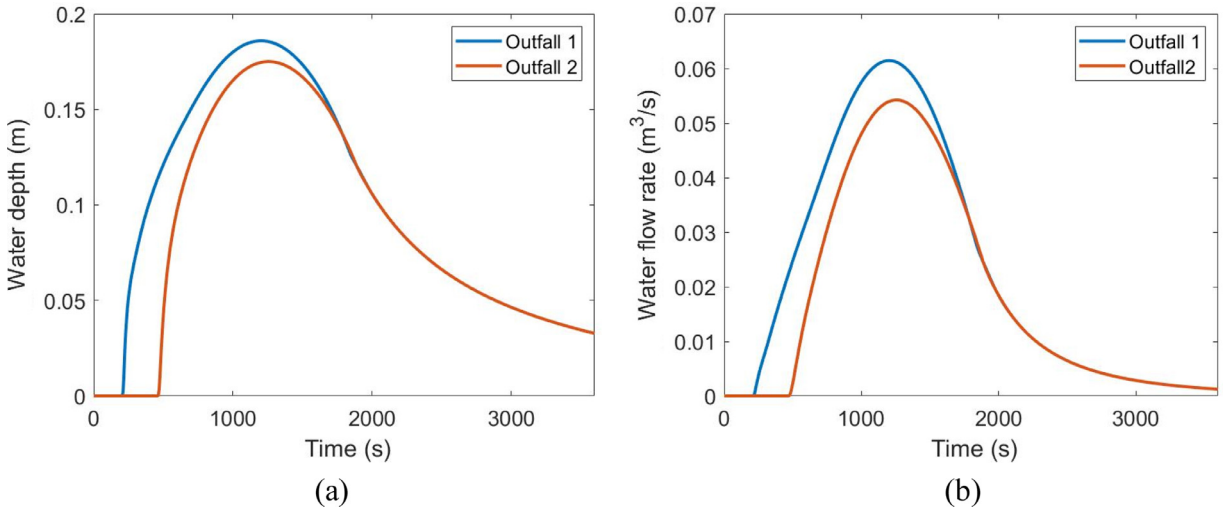

Fig. 17. Predicted water depths and flow rates at Outfall 1 and Outfall 2: (a) water depth; (b) flow rate.

3.4. A hypothetical drainage network system

This final test case is considered to demonstrate the current model's capability in simulating flows in a more practical drainage network system. The hypothetical system is consisted of 24 pipes, 15 junctions and 2 outfalls that are set up to reflect a simple but practical urban drainage configuration. As illustrated in Fig. 15, the junctions and outfalls have different elevations, creating a slope to allow water to travel from the upstream inflow junction (Junction 1) to the downstream outfalls. A diameter of 0.5 m is used for all pipes, but the lengths of the pipes vary according to the network configuration, as detailed in Table 2. The pipes are discretized using 1 m uniform grids. The junctions have three different radiuses, i.e. 0.5 m, 0.6 m and 0.75 m, as detailed in Table 3. During the simulation, the Manning coefficient is set to 0.035 $m^{-1/3}$ s over the entire system. An inflow hydrograph as shown in Fig. 16 is imposed at Junction 1 to create a flow through the connecting pipes and junctions and finally discharging through Outfall 1 and Outfall 2.

Fig. 17 presents the simulation results in terms of water depth and flow rate at the two outfalls. Overall, the time histories of the outfall water depth and flow rate are consistent with the inflow hydrograph. Due to the shorter route between Junction 1 and Outfall 1, the flow arrives earlier at Outfall 1 than at Outfall 2; similarly, Outfall 1 welcomes the flood peak slightly earlier than Outfall 2. Both of the peak flow depth and discharge at Outfall 1 are higher than those at Outfall 2. To reach Outfall 2, the flow must travel longer and more complicated routes that involve more junctions and pipes, which will potentially lead to more complex flow hydrodynamics involving more momentum exchange and dissipation, and subsequently lower peaks of the water depth and flow rate. The inflow peaks before $t = 1000$ s and terminates at $t = 1800$ s and the simulation results clearly reflect the inflow pattern. This indicates reasonable prediction and demonstrates the capability of the current model in predicting flow hydrodynamics in practical drainage systems involving wet-dry fronts, complex junction-pipe-outfall connections and dynamic flow transitions.

4. Conclusions

This paper presents a novel 1D-2D coupled model for hydrodynamic simulation of transient flows in drainage networks. The model adopts a 1D TPA model to simulate the flow dynamics in pipes, which can effectively capture free-surface and pressurized transient flows. For the junction calculations, an innovative approach that treats a junction as a 2D domain is proposed, with the flow hydrodynamics in the junction calculated using a 2D SWE model to automatically take into account both mass and momentum conservation. The 2D junction calcutation approach is further implemented with a new method for evaluating the pressure fluxes over the wall interface. Finally, the two modelling components are dynamically coupled together to become an integrated drainage model, which is validated against one experimental and three idealized test cases with satisfactory results. In one of the test cases, the numerical predictions are also compared with the results neglecting momentum exchange inside the junctions to demonstrate the importance of reinforcing momentum conservation in the junction calculations.

In conclusion, the proposed drainage model provides a potential tool for accurate simulation of transient flow hydrodynamics in urban drainage systems and has the following technical highlights:

1. The presented drainage model adopts a 2D numerical method for the junction flow calculations, which introduces a momentum-based approach to automatically account for momentum exchange in multi-pipe junctions with arbitrary entrance and exit angles.
2. The model formulation streamlines the enforcement of boundary conditions between pipes and junctions, effectively removing the requirement of numerous logical checks based on the possibility of either pressurized or free surface flow in the previously developed models (e.g. Sanders and Bradford, 2010).
3. Implemented with a finite volume shock-capturing scheme and robust source term discretization methods, the drainage model gives relatively smooth and stable predictions of complex flow that involves wet-dry fronts and dynamic transition between free surface and pressurized flows in pipe networks of moderate complexity. This demonstrates the model's potential for wider application in large-scale urban drainage modelling.

Declaration of Competing Interest

On behalf of all of the authors of the above paper being submitted to Advances in Water Resources, I confirm that there is no conflict of interest has been identified or raised for this submission.

CRediT authorship contribution statement

Qian Li: Conceptualization, Methodology, Validation, Visualization, Writing - original draft. **Qiuhua Liang:** Supervision, Funding acquisition, Conceptualization, Methodology, Writing - review & editing. **Xilin Xia:** Supervision, Funding acquisition, Conceptualization, Methodology.

Acknowledgments

This work was funded by the UK Natural Environment Research Council (NERC) through the FUTURE-DRAINAGE project (NE/S016678/1) and the Royal Academy of Engineering through a Newton Fund research grant (UUFRIP\100033) as part of the UK-China Urban Flooding Research Impact Programme. The first author thanks the financial support provided by the China Scholarship Council Scholarship. The authors also thank Prof. Brett F. Sanders and other two anonymous reviewers for their constructive comments.

Supplementary materials

Supplementary material associated with this article can be found, in the online version, at doi:10.1016/j.advwatres.2020.103519.

References

Bermúdez, A., López, X., Vázquez-Cendón, M.E., 2017. Treating network junctions in finite volume solution of transient gas flow models. J. Comput. Phys. 344, 187–209. https://doi.org/10.1016/j.jcp.2017.04.066.

Beg, M.N.A., Carvalho, R.F., Tait, S., Brevis, W., Rubinato, M., Schellart, A., Leandro, J., 2017. A comparative study of manhole hydraulics using stereoscopic PIV and different RANS models. Water Sci. Technol. 87–98. https://doi.org/10.2166/wst.2018.089.

Beg, M.N.A., Carvalho, R.F., Leandro, J., 2018. Effect of surcharge on gully-manhole flow. J. Hydro Environ. Res. 19, 224–236. https://doi.org/10.1016/j.jher.2017.08.003.

Borsche, R., Klar, A., 2014. Flooding in urban drainage systems: coupling hyperbolic conservation laws for sewer systems and surface flow. Int. J. Numer. Methods Fluids 76 (11), 789–810. https://doi.org/10.1002/fld.3957.

Bousso, S., Daynou, M., Fuamba, M., 2012. Numerical modeling of mixed flows in storm water systems: critical review of literature. J. Hydraul. Eng. 139 (4), 385–396. https://doi.org/10.1061/(asce)hy.1943-7900.0000680.

Burger, G., Sitzenfrei, R., Kleidorfer, M., Rauch, W., 2014. Parallel flow routing in SWMM 5. Environ. Model. Softw. 53, 27–34. https://doi.org/10.1016/j.envsoft.2013.11.002.

Chang, T.J., Wang, C.H., Chen, A.S., 2015. A novel approach to model dynamic flow interactions between storm sewer system and overland surface for different land covers in urban areas. J. Hydrol. 524, 662–679. https://doi.org/10.1016/j.jhydrol.2015.03.014.

Capart, H., Sillen, X., Zech, Y., 1997. Numerical and experimental water transients in sewer pipes. J. Hydraul. Res. 35 (5), 659–672. https://doi.org/10.1080/00221689709498400.

Capart, H., Bogaerts, C., Kevers-Leclercq, J., Zech, Y., 1999. Robust numerical treatment of flow transitions at drainage pipe boundaries. Water Sci. Technol. 39 (9), 113–120. https://doi.org/10.1016/s0273-1223(99)00307-8.

Cunge, J.A., Holly, F.M., Verwey, A., 1980. Practical Aspects of Computational River Hydraulics. Pitman, London, p. 420.

Franzini, F., Hoedenaeken, D., Soares-Frazão, S., 2018. Modeling the flow around islands in rivers using a one-dimensional approach. In: Gourbesville, P., Cunge, J., Caignaert, G. (Eds.), Advances in Hydroinformatics. Springer Water Springer, Singapor. https://doi.org/10.1007/978-981-10-7218-5_9.

Harten, A., Lax, P.D., Leer, B.V., 1983. On upstream differencing and Godunov-type schemes for hyperbolic conservation laws. SIAM Rev. 25 (1), 35–61. https://doi.org/10.1007/978-3-642-60543-7_4.

Herty, M., Seaïd, M., 2008. Simulation of transient gas flow at pipe-to-pipe intersections. Int. J. Numer. Methods Fluids 56 (5), 485–506. https://doi.org/10.1002/fld.1531.

Hong, S.W., Kim, C., 2011. A new finite volume method on junction coupling and boundary treatment for flow network system analyses. Int. J. Numer. Methods Fluids 65 (6), 707–742. https://doi.org/10.1002/fld.2212.

Hsu, M.H., Chen, S.H., Chang, T.J., 2000. Inundation simulation for urban drainage basin with storm sewer system. J. Hydrol. 234 (1-2), 21–37. https://doi.org/10.1016/s0022-1694(00)00237-7.

Li, J., McCorquodale, A., 1999. Modeling mixed flow in storm sewers. J. Hydraul. Eng. 125 (11), 1170–1180. https://doi.org/10.1061/(asce)0733-9429(1999)125:11(1170).

León, A.S., Ghidaoui, M.S., Schmidt, A.R., García, M.H., 2006. Godunov-type solutions for transient flows in sewers. J. Hydraul. Eng. 132 (8), 800–813. https://doi.org/10.1061/(asce)0733-9429(2006)132:8(800).

León, A.S., Ghidaoui, M.S., Schmidt, A.R., Garcia, M.H., 2010a. A robust two-equation model for transient-mixed flows. J. Hydraul. Res. 48 (1), 44–56. https://doi.org/10.1080/00221680903565911.

León, A.S., Liu, X., Ghidaoui, M.S., Schmidt, A.R., García, M.H., 2010b. Junction and drop-shaft boundary conditions for modeling free-surface, pressurized, and mixed free-surface pressurized transient flows. J. Hydraul. Eng. 136 (10), 705–715. https://doi.org/10.1061/(asce)hy.1943-7900.0000240.

Leandro, J., Martins, R., 2016. A methodology for linking 2D overland flow models with the sewer network model SWMM 5.1 based on dynamic link libraries. Water Sci. Technol. 73 (12), 3017–3026. https://doi.org/10.2166/wst.2016.171.

McCorquodale, J., Hamam, M., 1983. Modeling surcharged flow in sewers. In: Proceedings of the International Symposium on Urban Hydrology, Hydraulics and Sediment Control, Lexington, Kentucky. University of Kentucky, pp. 331–338.

Malekpour, A., Karney, B., 2014. A non-oscillatory preissmann slot method based numerical model. Proc. Eng. 89, 1366–1373. https://doi.org/10.1016/j.proeng.2014.11.461.

Maranzoni, A., Dazzi, S., Aureli, F., Mignosa, P., 2015. Extension and application of the Preissmann slot model to 2D transient mixed flows. Adv. Water Resour. 82, 70–82. https://doi.org/10.1016/j.advwatres.2015.04.010.

Noh, S.J., Lee, S., An, H., Kawaike, K., Nakagawa, H., 2016. Ensemble urban flood simulation in comparison with laboratory-scale experiments: impact of interaction models for manhole, sewer pipe, and surface flow. Adv. Water Resour. 97, 25–37. https://doi.org/10.1016/j.advwatres.2016.08.015.

Noh, S.J., Lee, J.H., Lee, S., Kawaike, K., Seo, D.J., 2018. Hyper-resolution 1D-2D urban flood modelling using Lidar data and hybrid parallelization. Environ. Model. Softw. 103, 131–145. https://doi.org/10.1016/j.envsoft.2018.02.008.

Preissmann, A., 1961. Propagation des intumescences dans lescanaux et rivieres. In: Proceedings of the First Congress French Association for Computation, Grenoble.

Politano, M., Odgaard, A.J., Klecan, W., 2007. Case study: numerical evaluation of hydraulic transients in a combined sewer overflow tunnel system. J. Hydraul. Eng. 133 (10), 1103–1110. https://doi.org/10.1061/(asce)0733-9429(2007)133:10(1103).

Sanders, B.F., Bradford, S.F., 2010. Network implementation of the two-component pressure approach for transient flow in storm sewers. J. Hydraul. Eng. 137 (2), 158–172. https://doi.org/10.1061/(asce)hy.1943-7900.0000293.

Schmitt, T.G., Thomas, M., Ettrich, N., 2005. Assessment of urban flooding by dual drainage simulation model Risursim. Water Sci. Technol. 52 (5), 257–264. https://doi.org/10.2166/wst.2005.0141.

Trajkovic, B., Ivetic, M., Calomino, F., D'Ippolito, A., 1999. Investigation of transition from free surface to pressurized flow in a circular pipe. Water Sci. Technol. 39 (9), 105–112. https://doi.org/10.1016/s0273-1223(99)00222-x.

Vasconcelos, J.G., Wright, S.J., Roe, P.L., 2006. Improved simulation of flow regime transition in sewers: two-component pressure approach. J. Hydraul. Eng. 132 (6), 553–562. https://doi.org/10.1061/(asce)0733-9429(2006)132:6(553).

Vasconcelos, J.G., Wright, S.J., 2007. Comparison between the two-component pressure approach and current transient flow solvers. J. Hydraul. Res. 45 (2), 178–187. https://doi.org/10.1080/00221686.2007.9521758.

Wiggert, D.C., 1972. Transient flow in free-surface, pressurized systems. J. Hydraul. Div. 98 (1), 11–27.

Xia, X., Liang, Q., 2018. A new efficient implicit scheme for discretising the stiff friction terms in the shallow water equations. Adv. Water Resour. 117, 87–97. https://doi.org/10.1016/j.advwatres.2018.05.004.